Supporting Information: Low-Dimensional Quantum Spin System Separated by Charge-Disproportionated Nonmagnetic BEST Layers in $(BEST)_3Zn(NCS)_4$

Hiroki Shiibashi[†],[a] Takuya Kobayashi[*],[b,c] and Hiromi Taniguchi[b]

[a]*Faculty of Science, Saitama University, Saitama 338-8570, Japan*

[b]*Graduate School of Science and Engineering, Saitama University, Saitama, 338-8570, Japan*

[c]*Research and Development Bureau, Saitama University, Saitama 338-8570, Japan*

Overlap integrals of $(BEST)_3Zn(NCS)_4$

The intermolecular overlap integrals S were calculated by the extended Hückel method.[S1] The ζ exponent and ionization potential (in eV) for the atomic orbitals were taken from the literature[S2,S3] as follows: Se : 4s 2.44 (-20.0), 4p 2.07 (-10.8), 4d 1.5 (-5.44); S : 3s 2.122 (-20.0), 3p 1.827 (-11.0), 3d 1.5 (-5.44); C : 2s 1.625 (-21.4), 2p 1.625 (-11.4); H : 1s 1.3 (-13.6).

Figures S1(a) and S1(c) show the crystal structure viewed along the molecular long axis and its schematic representation, respectively, together with definitions of the overlap integrals. Four crystallographically independent donor molecules stack approximately along the [110] direction. All relevant intermolecular contacts within layer I can be described by the set of overlaps along

[†]Present address: Graduate School of Medical Sciences, Kanazawa University, Kanazawa 920-8640, Japan

[*]E-mail: tkobayashi@mail.saitama-u.ac.jp

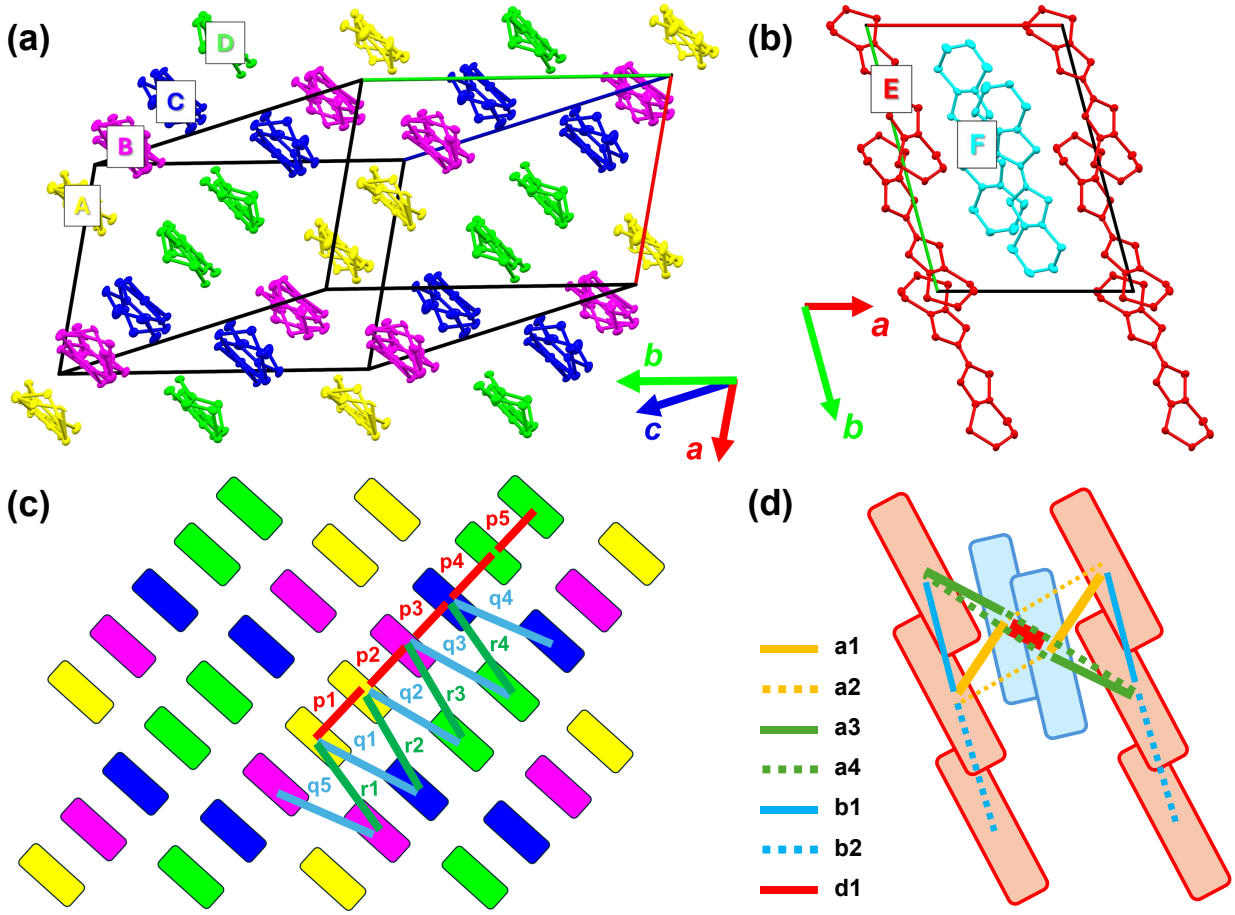

Figure S1: Arrangement of BEST molecules and definitions of intermolecular overlap integrals in layers I [(a),(c)] and III [(b),(d)].

the stacking direction (p1–p5) and those between adjacent stacks (q1–q5 and r1–r4), as labeled in Fig. S1(c). The values are listed in Table S1.

Table S1: Intermolecular overlap integrals S within layer I: p1–p5 are parallel to the stacking direction; q1–q5 and r1–r4 are interstack overlaps between adjacent stacks. The notations are given in Fig. S1(c).

Mode	S (10^{-3})	Mode	S (10^{-3})	Mode	S (10^{-3})
p1	38.40	q1	−5.29	r1	2.77
p2	−23.51	q2	−10.64	r2	4.90
p3	12.74	q3	4.91	r3	−0.42
p4	24.59	q4	2.57	r4	−3.77
p5	36.28	q5	2.34		

Overlap integrals along the stack are larger than those between stacks, indicating a pronounced one-dimensional character in layer I. Among the intrastack contacts, the largest overlaps (p1 and p5) occur for symmetry-related pairs, A–A and D–D, consistent with electronic dimerization.

Table S2: Intermolecular overlap integrals S along the E-molecule chain (b1, b2), within the F-molecule dimer (d1), and between the chain and the dimer (between molecules E and F, a1–a4). The notations are given in Fig. S1(d).

Mode	S (10^{-3})	Mode	S (10^{-3})
a1	−10.86	b1	−0.86
a2	−0.07	b2	0.33
a3	−6.33	d1	21.76
a4	1.70		

Figures S1(b) and S1(d) display the crystal structure of layer III and a schematic representation, respectively. Here we define the overlap integrals along the E-molecule chain (b1, b2), within the F-molecule dimer (d1), and between molecules E and F (a1–a4) as shown in Fig. S1(d). The values are listed in Table S2. The F–F overlap (d1) is the largest within layer III, supporting dimerization of molecules F. Along the long axis of molecule E, there are two distinct overlaps b1 and b2, through the terminal fragment. Because molecule E lies on a general position in $P\bar{1}$, these contacts are not symmetry equivalent. The overlap integrals between E and F also contain several finite paths (a1–a4), with a1 and a3 being the next largest following d1.

Estimates of exchange couplings

Here we briefly discuss possible exchange paths between the localized spins in molecule E and estimate the exchange couplings. This discussion provides order-of-magnitude estimates and does not uniquely determine the microscopic exchange topology. First, we estimate the possible intrachain exchange interaction within the chain-like arrangement of molecule E nearly parallel to the molecular long axis (blue solid and dotted lines in Fig. S2). The exchange interaction J can be expressed as $2J = 4t^2/U$, where t and U represent the intermolecular transfer integral and the on-site Coulomb interaction on a molecule, respectively. Transfer integrals along the b axis were estimated to be $t_{b1} \approx 8.6$ meV and $t_{b2} \approx 3.3$ meV from the relation $t = ES$, where E is the energy level of the highest occupied molecular orbital taken as $E = -10$ eV. The on-site Coulomb interaction of BEDT-TTF has been estimated to be $U \approx 4$ eV.[S4] In addition, the difference between the first and second oxidation potentials ($\Delta E = E_1 - E_2$), which is a measure of the on-site Coulomb interaction, is comparable between ET and BEST molecules.[S5,S6] Therefore, we adopted the same value for BEST. Using the above values, the intrachain interaction J is estimated to be on the order of 10^{-1} K. This estimate is far smaller than the magnitude extracted from the susceptibility fit ($J \approx 36$ K), indicating that direct E–E coupling alone cannot account for the observations. It should be emphasized, however, that the Hückel parameters used in extended Hückel calculations are empirical,[S2] and the present estimates may therefore be subject to systematic uncertainties; in particular, the Se electron density within the BEST molecule could be underestimated in the current parameterization.

We next consider the superexchange interaction mediated by the nonmagnetic F dimer. Treating the two molecules F as a dimer, the network of the effective E–(F dimer)–E interactions can be approximately regarded as a quasi-one-dimensional effective network nearly parallel to the a axis (yellow, green and red lines in Fig. S2). These interactions can be written as $t_{i-j} \sim t_i t_j/\Delta$,[S7] where t_i and t_j denote the transfer integrals between E molecule and F dimer, and Δ is the charge-transfer energy from molecule E to the closed-shell F dimer. The antiferromagnetic superexchange is then approximated as $2J_{i-j} \sim 4t_{i-j}^2/U \sim 4t_i^2 t_j^2/(\Delta^2 U)$.[S8] In the present case, we take Δ to be intradimer

transfer integral, t_{d1}, proportional to the bonding–antibonding splitting, and t_i (t_j) to be $t_{a1}/\sqrt{2}$ or $t_{a3}/\sqrt{2}$, as an order-of-magnitude estimate. Thus, the two dominant superexchange couplings J_{a1-a1} and J_{a1-a3} can be written as $J_{a1-a1} \sim t_{a1}^4/(2\,t_{d1}^2 U)$, $J_{a1-a3} \sim t_{a1}^2 t_{a3}^2/(2\,t_{d1}^2 U)$, respectively. Using the calculated overlap integrals in Table S2, J_{a1-a1} and J_{a1-a3} are estimated to be approximately 5 K and 1 K, respectively, which are not far from the estimate obtained from the analysis of the magnetic susceptibility. A quantitative determination of the exchange network and the appropriate minimal spin model will require first-principles calculations (e.g., t_{ij} based on Wannier functions, and screened U using the constrained random-phase approximation).

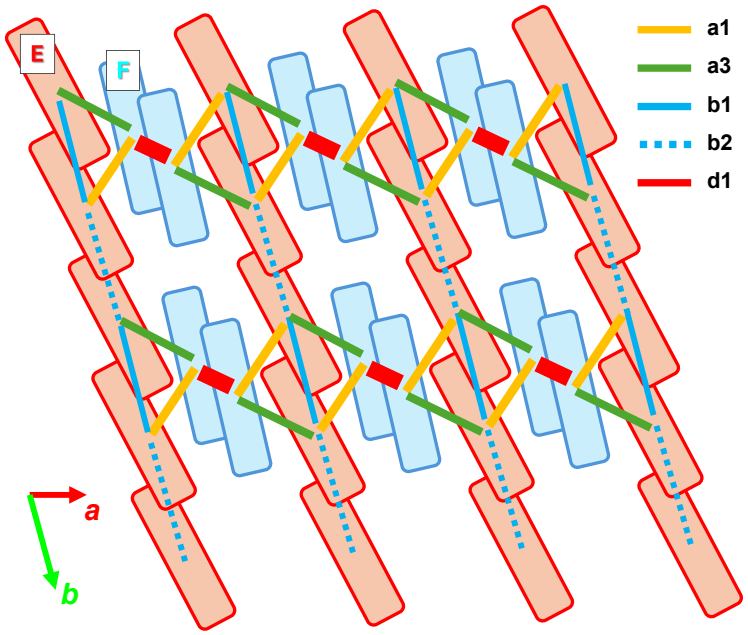

Figure S2: Schematic view of layer III highlighting the arrangement of molecules E and F and the dominant intermolecular overlap integrals. For clarity, a2 and a4 are omitted.

Magnetic-field dependence of spin susceptibility at low temperatures

To investigate the ground state of the present material, spin susceptibility measurements were performed under different magnetic fields using a SQUID magnetometer. In this experiment, a

sample (labeled as #2) different from that shown in the main text (#1) was measured; the two samples were independently synthesized. As shown in Fig. S3(a), the susceptibilities of the two samples reproduce each other well above 20 K, whereas an increase in the susceptibility is observed only for sample #2 at lower temperatures. This increase is attributed to paramagnetic impurities, which may not affect the magnetic-field dependence of the spin susceptibility in the low field region.

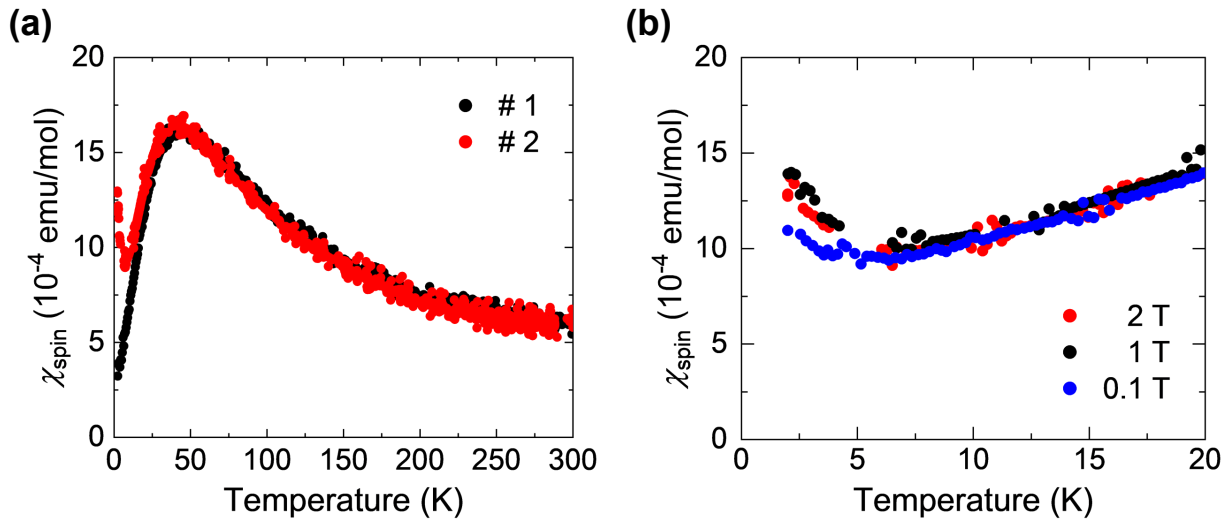

Figure S3: Temperature dependence of magnetic susceptibility at low temperatures for (a) different sample batches and (b) measured under different magnetic fields. In (a), the sample #1 represents the data presented in the main text, while sample #2 represents the data obtained from an independently synthesized polycrystalline sample.

Figure S3(b) shows the temperature dependence of spin susceptibility for sample #2, measured under the magnetic fields indicated in the figure. The data at 2 T are almost identical to those at 1 T, whereas a slightly lower susceptibility was observed at 0.1 T below $\sim$ 7 K, suggesting a possible magnetic ordering. Interchain interactions may become significant at low temperatures. To determine the ground states, further investigation using microscopic measurements is desirable.

References

(S1) Mori, T.; Kobayashi, A.; Sasaki, Y.; Kobayashi, H.; Saito, G.; Inokuchi, H. The Intermolecular Interaction of Tetrathiafulvalene and Bis(ethylenedithio)tetrathiafulvalene in Organic Metals. Calculation of Orbital Overlaps and Models of Energy-band Structures. *Bulletin of the Chemical Society of Japan* **1984**, *57*, 627–633.

(S2) Mori, T.; Katsuhara, M. Estimation of πd-Interactions in Organic Conductors Including Magnetic Anions. *Journal of the Physical Society of Japan* **2002**, *71*, 826–844.

(S3) Ito, A.; Kobayashi, T.; Sari, D. P.; Watanabe, I.; Saito, Y.; Kawamoto, A.; Tsunakawa, H.; Satoh, K.; Taniguchi, H. Antiferromagnetic ordering of organic Mott insulator λ-(BEDSe-TTF)$_2$GaCl$_4$. *Physical Review B* **2022**, *106*, 045114.

(S4) Scriven, E.; Powell, B. J. Toward the parametrization of the Hubbard model for salts of bis(ethylenedithio)tetrathiafulvalene: A density functional study of isolated molecules. *The Journal of Chemical Physics* **2009**, *130*.

(S5) Lee, V. Y. Chemistry of organic metals: Synthesis of bis(diseleno alkyl)tetrathiafulvalene, mixed sulfur-selenium analogs of BEDT-TTF. *Synthetic Metals* **1987**, *20*, 161–167.

(S6) Hsu, S.-Y.; Chiang, L. Y. Synthesis of bis(oxydimethylene)tetrathiafulvalene (BODM-TTF) and BEDSe-TTF. *Synthetic Metals* **1988**, *27*, 651–656.

(S7) Anderson, P. W. Antiferromagnetism. Theory of Superexchange Interaction. *Physical Review* **1950**, *79*, 350–356.

(S8) Imada, M.; Fujimori, A.; Tokura, Y. Metal-insulator transitions. *Reviews of Modern Physics* **1998**, *70*, 1039–1263.